Stimulated emission depletion microscopy for imaging of engineered and biological nanostructures

Christian Schumann, Christian Cavelius, Sabrina Schübbe and Annette Kraegeloh

Abstract

The investigation of interactions between engineered nanostructures and biological systems is a key component in the assessment of potential environmental and health implications due to the increasing application of nanotechnology. Combining the high specificity of bioconjugate fluorescence labeling techniques with the sub-diffraction resolution of Stimulated Emission Depletion (STED) microscopy and state-of-the-art nonlinear image restoration allows the imaging of these interactions on the length scales demanded by the interaction partners. In this article, we give an overview of the experimental approach and discuss its implications on the biological interpretation of the resulting fluorescence micrographs.

Introduction

The ongoing development of new nanoscale materials raises the important question about their effects on human health and environmental implications [1]. The properties and technological applications of nanomaterials are intimately interwoven with dimensions on a nanometer and thus sub-cellular length scale. Their interaction with biological systems is dominated by their physicochemical properties, which strongly depend not only on their chemical composition, but also on a multitude of parameters including surface chemistry, morphology, etc. [2]. It has been shown that nanoparticles are in principle able to penetrate biological membranes and enter biological cells, but the nature of this cellular uptake, as

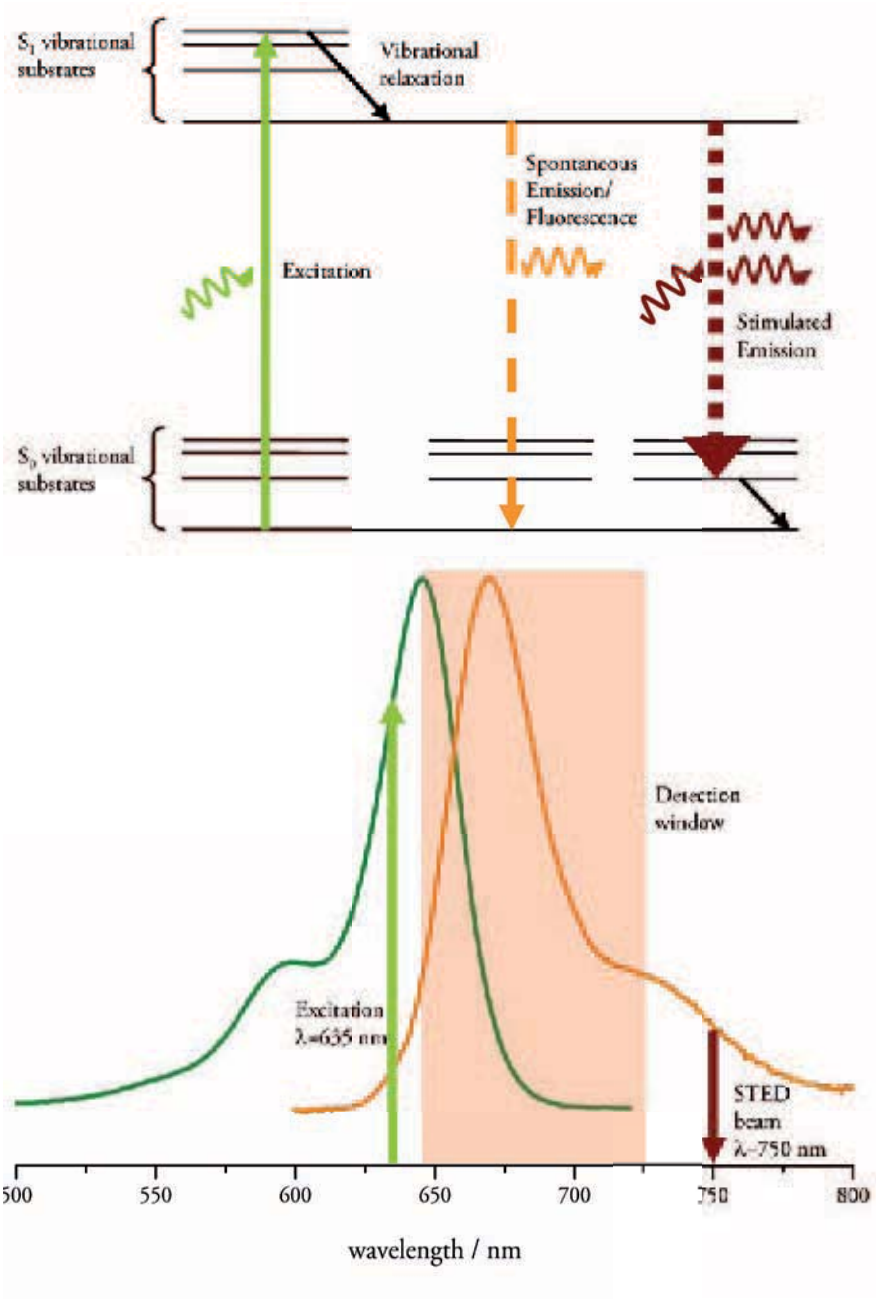

Figure 1: Top: molecular scheme of the STED process: After excitation to the S1 state and vibrational relaxation, fluorescence is suppressed by depopulation of the S1 state using stimulated emission in a pattern confining the center of the excitation spot. Bottom: Spectral realization for the STED-compatible dye Atto647N. The detection window is located between excitation and STED laser lines.

well as the mechanisms that determine the subcellular localization, the interaction with cellular components and finally the cellular response, are still unclear and subject to widespread research.

In our research, we seek to elucidate the transmembrane and intracellular transport processes of nanoparticles in human cells and to identify their biological interaction partners on a molecular level. In order to achieve this goal, we apply an imaging approach based on stimulated emission depletion (STED) microscopy, which enables us to visualize the interactions between engineered and biological structures with a spatial resolution beyond the optical diffraction limit.

Experimental

Imaging: All fluorescence imaging was performed on a Leica TCS SP5-STED (Leica Microsystems, Mannheim, Germany) using a Leica HCX PL APO 100x/1.4 oil objective. Excitation for STED imaging is accomplished by a picosecond diode laser (Picoquant, Berlin) with a wavelength of 635 nm. For point spread function (PSF) determination, confocal stacks with a pinhole size of 0.5 Airy units were recorded from samples of appropriate sub-resolution sized fluorescent beads (Invitrogen, Karlsruhe, Germany). PSFs were reconstructed by deconvolution of the image stacks with spherical object models. Biological specimens and PSF reference samples were mounted in FluorSave (CalBioChem, Merck, Darmstadt, Germany).

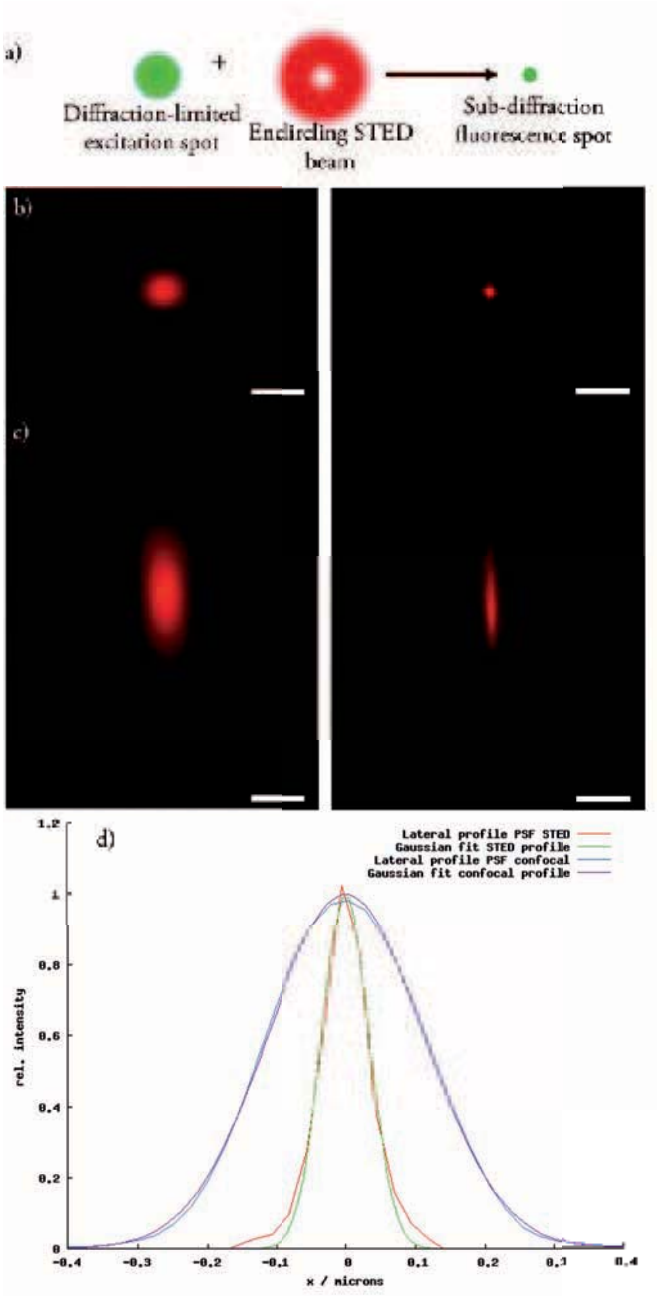

Figure 2: a) Lateral beam alignment of excitation and STED laser. Depopulation of the S_1 state by a STED laser spot with a node at the center of the excitation spot effectively reduces the size of the fluorescence spot scanned across the specimen. b) Lateral sections of the confocal (left) and STED (right) PSF, scale bar 500 nm. c) Axial sections of the confocal and STED PSFs, scale bar 500 nm. d) Lateral section profiles and gaussian fits of the STED and confocal PSFs. FWHM is 80 ± 3 nm (STED) and 264 ± 2 nm (confocal).

Image processing: Deconvolution of fluorescence micrographs was carried out using Huygens Professional (SVI, Hilversum, Netherlands) and custom written code in MATLAB (Mathworks, Natick, MA, USA).

STED confocal fluorescence microscopy

The idea of fluorescence microscopy is to excite a fluorescent dye by visible light (e. g. by a laser beam) to the S_1 state and detect the red-shifted fluorescence light that is emitted by its electronic relaxation back to the S_0 ground state [3]. The underlying physical process is spontaneous emission after vibrational relaxation in the S_1 state, causing the Stokes shift to longer emission wavelengths. This method not only enables background-free signal detection, but also enables molecular specificity of the fluorescent labels by conjugating them to particular molecules or structures. Fluorescence microscopy is realized by a vast array of concepts, among which conventional confocal microscopy achieves 3D optical sectioning by introduction of a confocal pinhole aperture in the fluorescence detection pathway and point-scanning of the specimen [4].

However, conventional confocal microscopy is limited by optical diffraction of the excitation laser spot and the resulting emission spot on the sample. This diffraction limiting case yields a lateral resolution of $\Delta s \approx \lambda / 2\ N\ A$, where *I* is the emission wavelength of the fluorescent dye and NA

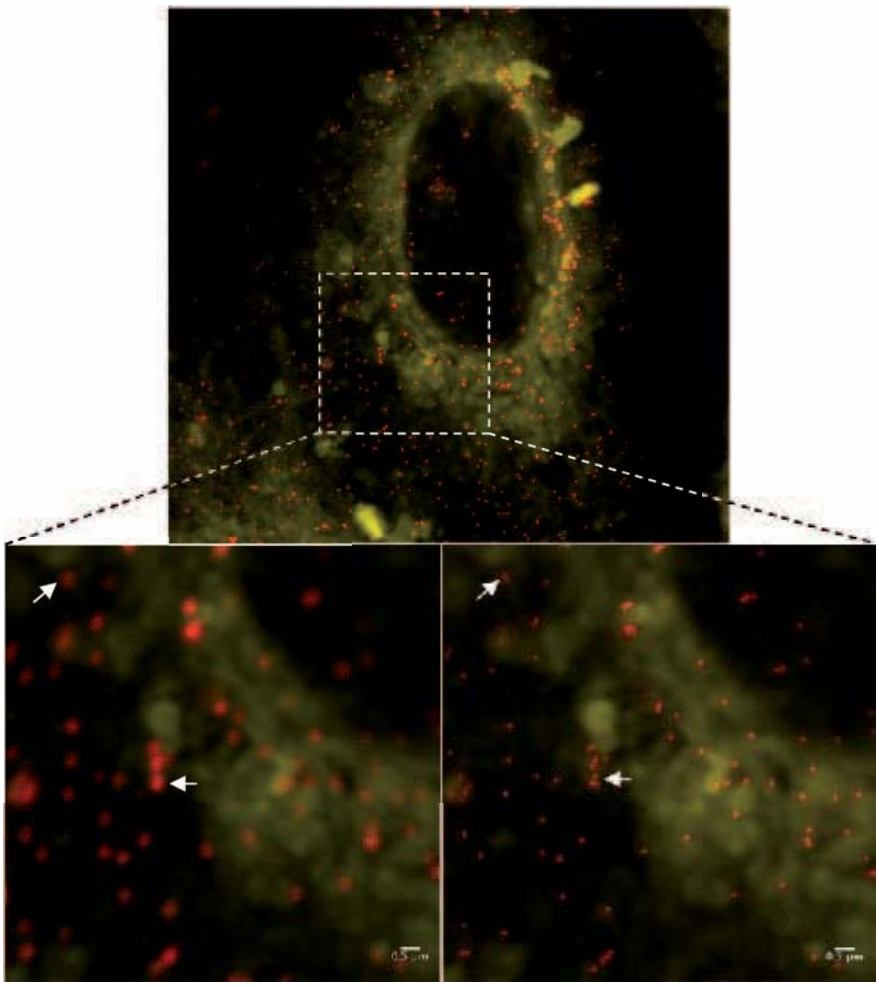

Figure 3: Top: A549 human lung epithelial cell (yellow: DiI membrane stain) after 24 h incubation with 130 nm diameter SiO2 nanoparticles (red). Bottom left: Zoom in using conventional confocal resolution. Bottom right: Same zoom area using STED. The arrows mark separation of sub-100 nm spaced particles not resolvable in standard confocal microscopy.

the numerical aperture of the microscope objective. Even with high-performance immersion objectives, the numerical aperture is limited. Furthermore, the use of light with a smaller wavelength for imaging induces ionization and is not compatible with sensitive biological specimens, leaving the diffraction barrier as the cen-

tral bottleneck for optical resolution in fluorescence microscopy.

The idea behind STED microscopy [5-7] is to confine the fluorescence emission spot on the specimen to a much smaller area than determined by diffraction by using the photophysical properties of the fluorescent marker. In the pulsed implementation used here, a short (picosecond) excitation laser pulse in the absorption spectrum of the dye is followed by an intense STED laser pulse in the red wing of the fluorescence spectrum that induces stimulated emission, and thus effectively depopulates the fluorescent S_1 state (Figure 1). In order for this scheme to induce a resolution enhancement, the depopulation is spatially located in a pattern encircling the center of the excitation spot (Figure 2a), and the photon flux of the STED laser is adjusted to saturate the transition from S_1 to S_0. The resulting optically induced, nonlinear deactivation of the fluorescence in the region covered by the STED laser yields a resolution enhancement which is theoretically only limited by the STED laser power applicable. The optical resolution in STED is given by $\Delta s \approx \lambda$ (2 N A $\sqrt{}$ 1+I / I_S) where I is the intensity of the depletion beam and I_s is the intensity required to reduce the fluorescence by half. The performance of the STED technique was quantified by 3D imaging of sub-resolution sized fluorescent beads. Lateral and axial sections through the resulting point spread functions (PSFs) reconstructed from the experimental data are depicted in Figure 2b and 2c, respectively. The experimentally determined lateral resolutions

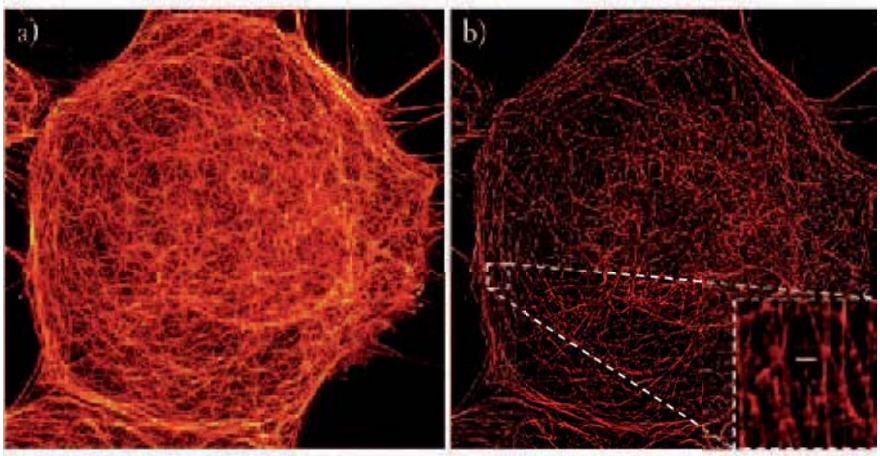

Figure 4: Nonlinear deconvolution of STED image data. a) Original data: Tubulin cytoskeleton of a Caco-2 colon epithelial cell, immunostained with Atto647N. b) Identical image after nonlinear deconvolution by wavelet-thresholded Landweber algorithm, regularization parameter 0.05. Inset: Zoom of indicated region, the FWHM (Gaussian fit) of the section profile of the marked filament is 55 ± 5 nm.

are 80 ± 3 nm for STED imaging as compared to 264 ± 2 nm in conventional confocal mode (Figure 2d). However, it should be noted that the axial resolution is unaffected by the STED implementation used, and is rather still diffraction limited (Figure 2c), where the optical resolution is given by $\Delta s \approx \lambda$ / N A. The central role of the fluorescent dye in the resolution enhancement puts spectral and kinetic compatibility requirements on its photophysical properties. Also, the combination of small pixel sizes and repetitive S_0-S_1 cycling of the dye by the laser pulse trains involved demands for excellent photostability. Furthermore, the reduced signal-to-noise ratio (SNR) of STED (see below) necessitates longer pixel dwell times and slightly higher excitation intensities. Finally, the desire for multidimensional recording (3D stacks, time series) requires extremely stable dyes compatible with the STED implementa-

tion present, for example Atto647N and Atto655.

The direct point-to-point imaging property of STED substantially differentiates this super-resolution technique from statistical methods like PALM [8] or STORM [9] and gives access to sensible time-resolved (live cell) experiments [10]. Fixed-cell experiments, to demonstrate the applicability of STED microscopy on the investigation of nanoparticle-cell interactions, have already successfully shown the additional information gained by the increased resolution [11]. For example, the study of the agglomeration behavior of cell associated nanoparticles demands an experimental method that can resolve single particles while being able to precisely differentiate cellular components. As can be seen from Figure 3, STED microscopy is ideally suited to this range of applications, being able to separate single nanoparticles within agglomerates. Its compatibility with physiological sample conditions also opens the possibility of exploiting its superior resolution in live cell imaging [10; 12].

Nonlinear image restoration

The resolution enhancement by STED microscopy is achieved solely by exploiting the photophysical properties of the fluorescent dyes, and thus STED microscopy still can be viewed as a purely physical image formation process with the ability of defining and measuring its PSF. The most common approach of modeling the physical image formation process assumes a linear relationship, in which the object is convolved with the PSF of the imaging system with additional poisson-distributed photon noise, $f = h \otimes g + n$ with the image *f*, the PSF *h*, the object *g* and the unknown noise *n*. In order to recover the true object *g* from the detected image *f*, the convolution operation is to be reversed [13]. In signal processing terms, the limited resolution of the imaging system is equivalent with a band limited spatial frequency response. Thus, spatial high-frequency noise is strongly amplified in the inverse operation of the convolution, and a successful determination of an estimate for *g* requires additional constraints on the problem. This additional regularization differs among deconvolution methods.

Linear solutions to the regularized inverse problem apply least-square or smoothness constraints to the estimate for *g* and are easy and computationally efficient to implement [14]. These additional constraints increase the SNR of the image; however, linear deconvolution techniques are unable to restore spatial frequencies lost in the band limited imaging process, and are thus unable to increase resolution.

Nonlinear image reconstruction methods are based on iterative deconvolution steps and application of the regularization operator. The most widespread class of methods relies on regularization by maximum entropy methods to enforce smoothness of the solution [15; 16]. Additionally, recent developments in mathematical image processing brought forth methods based on wavelet domain

sparseness constraints [17-19], and hybrid methods have also been used [20]. In contrast to linear deconvolution, iterative nonlinear image reconstruction allows resolution enhancement. The increase in resolution is dominated by the regularization parameter balancing the data fitting and smoothness measures of the solution, the permissible range of which is determined by the signal-to-noise ratio (SNR) of the image.

Nonlinear deconvolution of fluorescence micrographs has been routinely applied to widefield fluorescence and confocal image stacks, but its application to STED images raises new challenges. It is especially important to choose an appropriate regularization parameter as a choice based on established methods [21], will result in smoothed solutions, effectively reducing the resolution gained by STED. Compared to conventional confocal microscopy, the resolution enhancement in STED is obtained at the expense of a reduced SNR, which is induced by the signal attenuation in the center of the fluorescent spot by residual STED beam light and the general increase of Poisson noise due to lower photon numbers per sampled Volume. Thus, special care has to be taken when manually adjusting the regularization parameter so that resolution is still increased while avoiding deconvolution artifacts. Examples of deconvolution results are depicted in Figure 4, which shows maximum projections of STED stacks of the immunostained tubulin cytoskeleton of Caco-2 human colon epithelial cells as original data and after deconvolution using a wavelet-thresholded Landweber algorithm [17; 18]. The noise reduction is clearly visible, and the resolution has been improved to approx. 60 nm (Figure 4b inset). Also, deconvolution can substantially increase the dynamic range of fluorescence micrographs, which leads to a visually darker appearance.

Outlook

The combination of STED microscopy with nonlinear image restoration gives access to a substantial increase in optical resolution while still maintaining physiological conditions for the cell model. Together with the potential of selectively labeling cellular components involved in the nanoparticle-cell interaction, it constitutes a powerful tool for the exploration of the molecular and cell-biological mechanisms that underlie the effects of nanoparticle exposure. The application of these tools to the controlled experimental conditions of an *in vitro* cell model interacting with thoughtfully engineered and well-characterized nanoparticles in fixed-cell and live-cell experiments promises substantial insight into endocytotic pathways and intracellular transport, as well as intracellular interactions of nanoparticles.

References

[1] G. Oberdörster, E. Oberdörster and J. Oberdörster, Environ. Health Perspect., 2005, 113, 823-839.

[2] A. E. Nel, L. Madler, D. Velegol, T. Xia, E. M. Hoek, P. Somasundaran, F. Klaessig, V. Castranova and M. Thompson, Nature Mater., 2009, 8, 543-557.

[3] J. R. Lakowicz, Principles of fluorescence spectroscopy, Springer, 2006.

[4] J. Pawley, Handbook of biological confocal microscopy, Springer, 2006.

[5] S. W. Hell, J. Wichmann, Opt. Lett., 1994, 19, 780-782.

[6] T. A. Klar, S. Jakobs, M. Dyba, A. Egner and S. W. Hell, Proc. Natl. Acad. Sci. U S A, 2000, 97, 8206-8210.

[7] S. W. Hell, Science, 2007, 316, 1153-1158.

[8] E. Betzig, G. H. Patterson, R. Sougrat, O. W. Lindwasser, S. Olenych, J. S. Bonifacino, M. W. Davidson, J. Lippincott-Schwartz and H. F. Hess, Science, 2006, 313, 1642-1645.

[9] M. J. Rust, M. Bates and X. Zhuang, Nature Methods, 2006, 3, 793-795.

[10] V. Westphal, S. O. Rizzoli, M. A. Lauterbach, D. Kamin, R. Jahn and S. W. Hell, Science, 2008, 320, 246-249.

[11] S. Schübbe, C. Cavelius, C. Schumann, M. Koch and A. Kraegeloh, Adv. Eng. Mat., 2010, accepted.

[12] B. Hein, K. I. Willig and S. W. Hell, Proc. Natl. Acad. Sci. U S A, 2008, 105, 14271-14276.

[13] M. Bertero and P. Boccacci, Introduction to inverse problems in imaging, Institue of Physics Publishing, 1998.

[14] A. N. Tikhonov and V. L. Arsenin, Solution of ill-posed problems, Winston & Sons, 1977.

[15] W. H. Richardson, J. Opt. Soc. Am., 1972, 62, 55-59.

[16] L. B. Lucy, Astronomical Journal, 1974, 79, 745-754.

[17] M. A. T. Figueiredo and R. D. Nowak, IEEE Trans. Im. Proc., 2003, 12, 906-916.

[18] I. Daubechies, M. Defrise and C. De Mol, Comm. Pure Appl. Math., 2004, 57, 1413-1457.

[19] C. Vonesch and M. Unser, IEEE Trans. Im. Proc., 2009, 18, 509-523.

[20] J. Boutet de Monvel, S. Le Calvez and M. Ulfendahl, Biophys. J., 2001, 80, 2455-2470.

[21] N. P. Galatsanos and A. K. Katsaggelos, IEEE Trans. Im. Proc., 1992, 1, 322-336.